



OPEN ACCESS

EDITED BY

Maodu Yan,
Institute of Tibetan Plateau Research,
Chinese Academy of Sciences (CAS),
China

REVIEWED BY

Vivek Walia,
National Center for Research on
Earthquake Engineering, Taiwan
Dongliang Liu,
Chinese Academy of Geological
Sciences (CAGS), China

*CORRESPONDENCE

Xiaocheng Zhou,
zhouxiaocheng188@163.com
Ying Li,
subduction6@hotmail.com

SPECIALTY SECTION

This article was submitted to
Geochemistry, a section of the journal
Frontiers in Earth Science

RECEIVED 09 August 2022

ACCEPTED 25 October 2022

PUBLISHED 16 January 2023

CITATION

Liu J, Zhou X, Li Y, He M, Li J, Dong J,
Tian J, Yan Y, Ouyang S and Liu F (2023),
Relationship between
hydrogeochemical characteristics of
hot springs and seismic activity in the
Jinshajiang fault zone, Southeast
Tibetan Plateau.
Front. Earth Sci. 10:1015134.
doi: 10.3389/feart.2022.1015134

COPYRIGHT

© 2023 Liu, Zhou, Li, He, Li, Dong, Tian,
Yan, Ouyang and Liu. This is an open-
access article distributed under the
terms of the [Creative Commons
Attribution License \(CC BY\)](https://creativecommons.org/licenses/by/4.0/). The use,
distribution or reproduction in other
forums is permitted, provided the
original author(s) and the copyright
owner(s) are credited and that the
original publication in this journal is
cited, in accordance with accepted
academic practice. No use, distribution
or reproduction is permitted which does
not comply with these terms.

Relationship between hydrogeochemical characteristics of hot springs and seismic activity in the Jinshajiang fault zone, Southeast Tibetan Plateau

Jie Liu¹, Xiaocheng Zhou^{2*}, Ying Li^{2*}, Miao He², Jingchao Li², Jinyuan Dong², Jiao Tian², Yucong Yan², Shupeiyang Ouyang² and Fengli Liu²

¹Shaanxi Earthquake Agency, Xi'an, China, ²United Laboratory of High-Pressure Physics and Earthquake Science, Institute of Earthquake Forecasting, CEA, Beijing, China

Significant anomalous hydrogeochemical changes in hot spring water are detected during strong seismic cycles. It is now necessary to clarify the relationship between tectonic movements, earthquakes and the evolution of hot springs. In this paper, laboratory analyses of major, trace elements, δD , $\delta^{18}O$ and $^{87}Sr/^{86}Sr$ values of 28 hot spring waters in the Jinshajiang fault zone (JSJFZ) in the northwestern boundary of the Sichuan-Yunnan block were conducted. The results showed that the primary source of water for JSJFZ hot springs was atmospheric precipitation. The geothermal reservoir temperature variation based on the silicon enthalpy mixing model ranged from 73 to 272°C. And the circulation depth range was 1.2–5.4 km. The segmentation characteristics of the $^{87}Sr/^{86}Sr$ values were related to the influence of source rocks on groundwater cycle processes. A conceptual model of the hydrologic cycle of hot springs explained the spatial distribution of earthquakes associated with tectonic movements. The Batang segment had the strongest water-rock reaction, the highest reservoir temperature and the deepest circulation depth; meanwhile, it was also an earthquake prone area. The fluid circulation of the JSJFZ corresponds well with the seismicity, which indicates that the hydrological characteristics of the hot spring water in a fracture zone play a crucial role in receiving information on seismic activity.

KEYWORDS

thermal spring, hydrogeochemistry, seismic activity, jinshajiang fault zone, southeast Tibetan plateau

1 Introduction

Underground water geochemistry has played an important role in inferring geotectonic activity. Hydrological effects occurring during strong earthquake cycles have been observed both recently and historically (Scholz et al., 1973; King, 1986; Linde et al., 1988; Thomas, 1988; Kitagawa et al., 1996; Wang et al., 2001; Jonsson et al., 2003; Yang et al., 2011; Li et al., 2014; Skelton, 2014; Yan et al., 2014; Yuce et al., 2014; Manga and Wang, 2015; Rosen et al., 2018; Martinelli and Tamburello, 2020; Nakagawa et al., 2020; Fu et al., 2021; Zhang et al., 2021; Zhou et al., 2021). Large, localized, and sustained fluid pressures could account for weakness of deep-seated fault (Fulton and Saffer, 2009). In particular, geothermal hot springs are important conduits for the discharge of deep source fluids to the surface. The hot springs in the deep-seated fault zone have deep circulation. Due to high temperature and strong water-rock interaction in deep-cycle process, they can dissolve different kinds of minerals, resulting in different geochemical

characteristics (Bo et al., 2015; Guo et al., 2014; Tian et al., 2021). Such changes are always considered to be beneficial for fault tectonic and seismic studies.

The Jinshajiang fault zone (JSJFZ) is located in the southeast of the Tibetan Plateau. It has unique advantages in studying the relationship between earthquake and hydrochemistry of hot springs. Firstly, its major faults cut deeply into the crust and even through the asthenosphere (Wang et al., 2018). Secondly, it is an earthquake-prone area that has been hit by several $M_s \geq 6$ earthquakes since records began. Among them, the largest earthquake was the Batang $M7\frac{1}{4}$ earthquake in 1870 (Li et al., 2014). Since then, several earthquakes swarms with $M_s \geq 6$ had occurred in this region. Recently, the small and intermediate seismic activities in Batang have been more active. More importantly, the Batang geothermal field is a significant part of the eastern Tibetan Plateau geothermal belt (Tang et al., 2017). It is the geothermal field with the highest reservoir temperature (200°C – 225°C) along the Sanjiang Orogenic belt, and it has experienced a deep cycle (Yi et al., 2021).

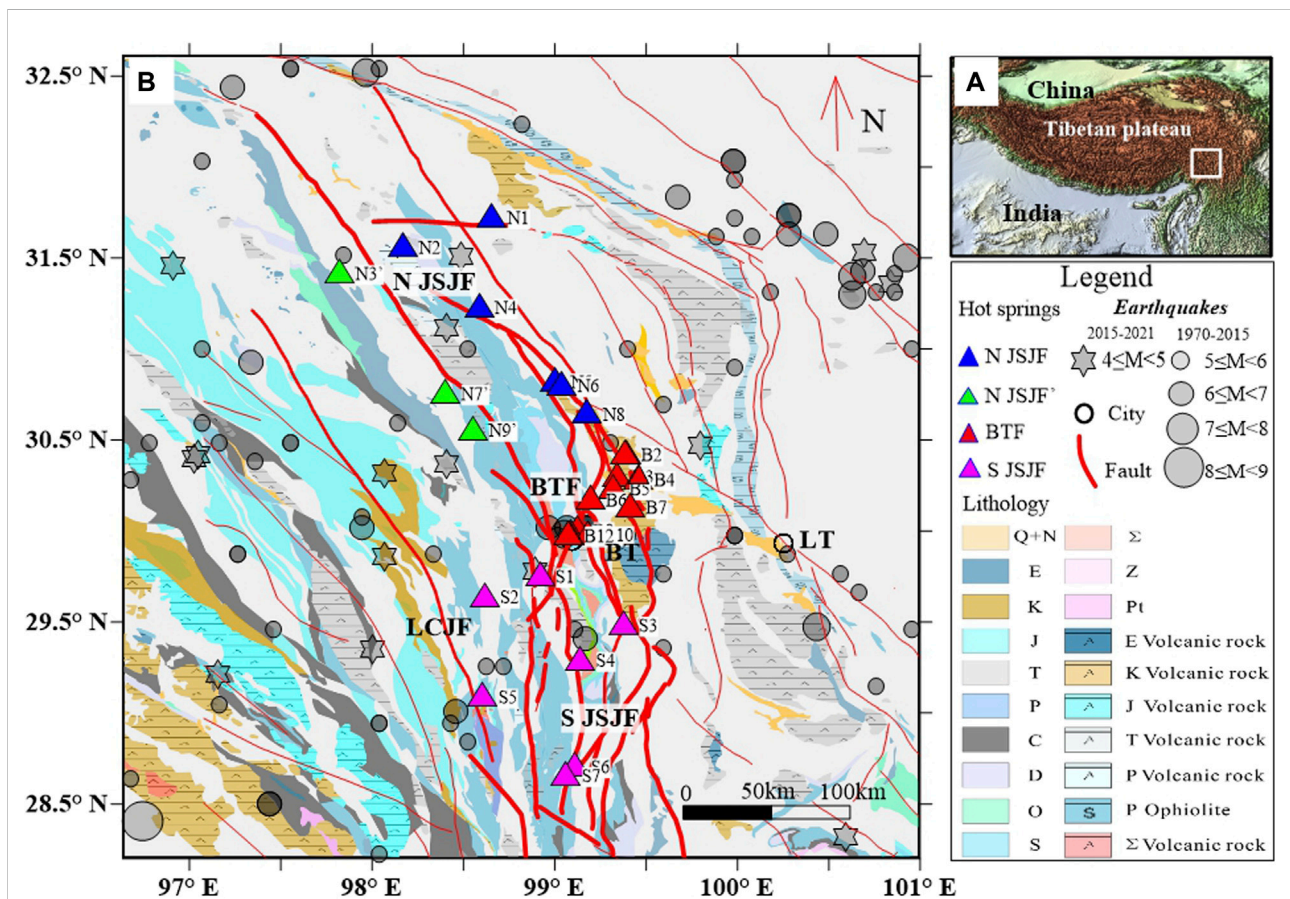


FIGURE 1 The plot of sampling site distribution. (A) Geological map showing the location of the study area. (B) Tectonic and tectonic and lithological features of the JSJFZ. Notes: The statistical earthquakes were divided into two parts, one is between 1970 and 2015 (grey circle), and the other is between 2015 and 2021 (grey polygon). The hot springs in the JSJFZ are divided into four parts (colored triangle). The background represents the lithology of the study area. The red line represents the fault.

TABLE 1 Geothermal water sampling sites information in the study area.

No	Segment	Longitude (°)	Latitude (°)	Altitude (m)	Sapmling time	Fault zone	Lithology and stratigraphic age
1	N1	98.66	31.69	3,285	2018.7.23	Northern JSJ fault	Limestone (T)
2	N2	98.17	31.52	3,994	2018.7.23	Northern JSJ fault	Sandstone, Mudstone, Volcanic rock (T)
3	N3'	97.83	31.38	4,107	2019.6.18	Northern JSJ fault	Limestone (T)
4	N4	98.59	31.20	2,906	2017.6.28	Northern JSJ fault	Limestone (T)
5	N5	99.00	30.80	2,945	2017.6.25	Northern JSJ fault	Limestone (T)
6	N6	99.04	30.78	2,964	2017.6.25	Northern JSJ fault	Limestone (T)
7	N7'	98.40	30.73	3,802	2019.6.17	Northern JSJ fault	Conglomerate, Sandstone, Mudstone (N)
8	N8	99.18	30.62	3,313	2018.7.21	Northern JSJ fault	Sandstone, Slate, limestone (T)
9	N9'	98.56	30.54	3,952	2019.6.17	Northern JSJ fault	Limestone (T)
10	B1	99.39	30.40	3,562	2019.6.15	BT Fault	Metamorphic clastic rock, limestone (T)
11	B2	99.38	30.40	3,562	2019.6.15	BT fault	Metamorphic clastic rock, limestone (T)
12	B3	99.34	30.28	3,287	2019.6.15	BT fault	Metamorphic sand slate, limestone (T)
13	B4	99.45	30.27	3,933	2019.6.15	BT fault	Metamorphic clastic rock, limestone (T)
14	B5	99.32	30.22	3,167	2016.4.26	BT fault	Carbonate rock (P)
15	B6	99.19	30.16	2,726	2019.6.15	BT fault	Metamorphic clastic rock, limestone (T)
16	B7	99.41	30.12	3,952	2019.6.16	BT fault	Metamorphic sand slate, limestone (T)
17	B8	99.12	29.99	2,668	2019.6.16	BT fault	Ophiolite group, limestone (P-T)
18	B9	99.08	29.98	2,517	2010.6.13	BT fault	Ophiolite group, limestone (P-T)
19	B10	99.18	29.97	3,079	2019.6.16	BT fault	Ophiolite group, limestone (P-T)
20	B11	99.08	29.97	2,519	2019.6.17	BT fault	Ophiolite group, limestone (P-T)
21	B12	99.07	29.96	2,513	2018.7.21	BT fault	Ophiolite group, limestone (P-T)
22	S1	98.92	29.74	2,646	2016.4.26	Southern JSJ fault	Ophiolite group, limestone (P-T)
23	S2	98.62	29.63	3,942	2018.7.22	Southern JSJ fault	Sandstone, Mudstone, Conglomerate (K)
24	S3	99.37	29.48	3,247	2017.6.26	Southern JSJ fault	Limestone (T)
25	S4	99.14	29.29	3,099	2017.6.26	Southern JSJ fault	Metamorphic clastic rock, limestone (T)
26	S5	98.61	29.09	2,655	2018.4.27	LCJ fault	Sandstone, Mudstone (J)
27	S6	99.11	28.71	3,270	2018.4.26	Southern JSJ fault	Carbonate rock (P)
28	S7	99.06	28.67	3,235	2018.4.26	Southern JSJ fault	Carbonate rock (P)

Previous studies have focused on the source of heat and chemical characteristics of some springs in this area (Shi and wang, 2017; Tang et al., 2017; Zhang, 2017; Hou et al., 2018; Tian et al., 2018, 2019; Zhou et al., 2020a; Yi et al., 2021; Liu et al., 2022). However, limited work has been reported on the relationship between the hydro-chemical characteristics of hot springs and fault activity. Such studies are important for evaluating the geothermal energy potential along the fracture zone. In this study, we focus on the hydrochemical properties and origin of 28 hot springs located in the JSJFZ. Major and trace elements, $^{87}\text{Sr}/^{86}\text{Sr}$ values, δD and $\delta^{18}\text{O}$ values are discussed to character the hydrochemical properties of these hot springs. Various methods were employed to calculate the reservoir temperature and depth of water circulation of these hot springs, so as to reveal their possible hydrochemical evolution processes. An attempt has been made to discuss the relationship between hot spring evolution and seismic activity through a conceptual

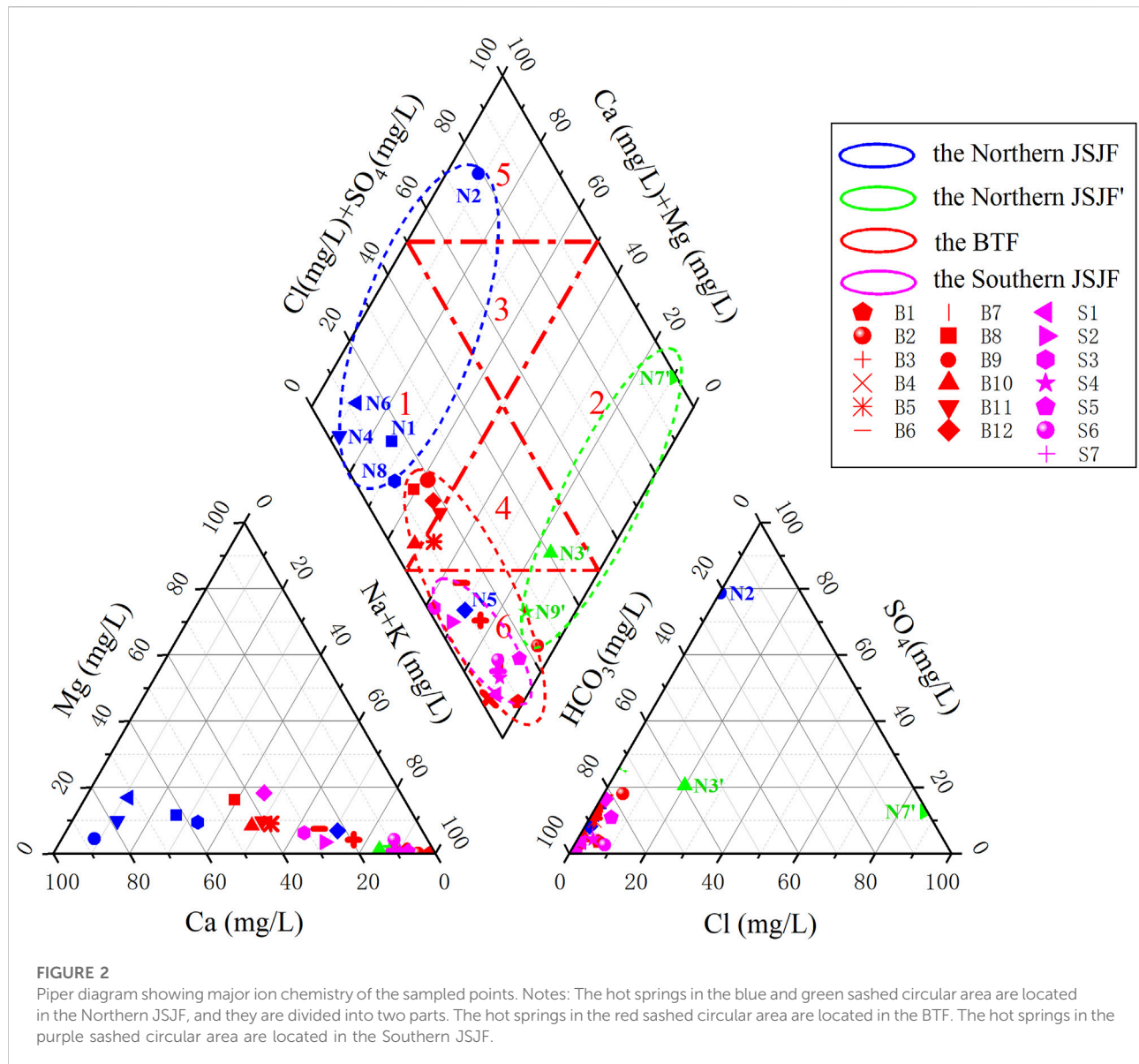
model of hot spring hydrology cycle, and prospect its implications for future monitoring.

2 Geological setting

The JSJFZ is located in the southeastern Tibetan Plateau, which has long been controlled by the NS compression due to the collision between the Indian and Eurasian continents (Yin and Harrison, 2003). Since the late Cenozoic, because of the rapid northward growth and episodic eastward extrusion of the Tibetan Plateau, the Sichuan-Yunnan diamond-shaped block (SYDSB) has become the main channel for the escape of plateau materials to the east and southeast (Zhu et al., 2017). The JSJFZ is part of the northwestern margin of the SYDSB (Figure 1A). It is a multi-stage active suture, and the faults in this area are mainly right-lateral strike-slip and thrust faults (Wang et al., 2018). Its general trend is NW-SE oriented distribution,

TABLE 2 Hydrochemical properties, major chemical constituents of the geothermal water samples.

Segment	T (°C)	pH	K+ (mg/L)	Na+(mg/L)	Ca2+(mg/L)	Mg2+(mg/L)	Cl- (mg/L)	SO42- (mg/L)	CO32- (mg/L)	HCO3- (mg/L)	SiO2 (mg/l)	TDS	Hydrochemical type
N1	15.80	7.77	3.68	27.06	72.15	13.54	2.57	46.50	26.40	234.85	18.40	310.13	HCO3-Ca•Na
N2	40.50	7.14	3.00	37.38	412.64	21.56	2.53	1115.43	29.04	269.07	44.30	1757.77	SO4•HCO3-Ca
N3'	58.80	7.74	38.02	511.06	91.53	7.71	292.21	301.89	90.08	782.25	68.27	1730.79	HCO3-Na
N4	33.00	6.57	3.92	40.97	298.45	37.83	5.81	22.57	—	953.89	27.39	888.46	HCO3-Ca
N5	48.50	7.22	52.36	369.16	131.88	41.33	15.58	116.52	—	1260.54	50.08	1365.63	HCO3-Na
N6	23.00	7.76	1.30	10.57	75.47	17.84	1.37	29.76	—	217.92	12.09	254.83	HCO3-Ca
N7'	10.57	7.37	78.60	12,979	1258.70	95.52	25,238	3708.77	64.63	107.66	9.10	43,542	Cl-Na
N8	35.20	7.05	12.21	80.99	161.85	26.97	2.99	74.57	56.10	597.86	30.82	717.55	HCO3-Ca•Na
N9'	73.80	8.25	13.61	301.41	40.09	6.33	8.87	212.29	91.45	562.04	93.30	959.21	HCO3-Na
B1	86.10	8.89	29.94	338.72	4.17	0.92	41.69	26.27	151.27	499.83	—	867.72	HCO3-Na
B2	82.00	8.57	14.34	240.10	12.02	0.34	31.27	115.19	—	488.00	323.14	673.19	HCO3-Na
B3	60.00	7.12	18.89	273.54	73.84	16.09	11.57	99.70	123.08	695.56	106.14	968.68	HCO3-Na
B4	65.80	7.32	19.80	258.94	27.50	1.47	12.87	4.21	92.14	611.68	90.31	732.70	HCO3-Na
B5	50.00	7.27	30.42	197.80	167.69	39.57	16.97	103.98	—	917.93	—	1018.01	HCO3-Na•Ca
B6	52.80	7.16	24.84	288.79	127.39	35.90	9.09	147.37	148.52	938.14	78.97	1254.35	HCO3-Na•Ca
B7	79.80	7.55	9.73	123.42	14.61	3.34	5.30	30.57	61.88	234.88	137.82	378.96	HCO3-Na
B8	36.40	7.13	11.33	99.48	124.90	45.53	3.24	104.45	102.45	540.37	41.94	763.46	HCO3-Ca•Na
B9	31.50	8.50	23.70	80.08	116.56	91.82	4.62	66.56	—	215.20	—	492.39	HCO3-Ca•Mg
B10	35.70	7.21	18.22	162.87	166.56	31.94	15.10	49.43	100.39	862.64	45.15	978.25	HCO3-Ca•Na
B11	46.40	7.69	27.58	153.11	146.97	35.71	11.50	163.55	47.44	770.36	52.43	974.48	HCO3-Na•Ca
B12	45.50	7.14	31.60	137.08	130.84	67.24	10.95	162.33	69.30	737.43	85.17	980.84	HCO3-Na•Ca
S1	56.50	7.85	10.87	261.44	22.02	2.02	9.89	22.95	—	625.86	—	647.54	HCO3-Na
S2	17.60	7.59	8.65	158.73	65.88	8.39	2.42	23.59	48.18	532.10	—	585.92	HCO3-Na•Ca
S3	45.00	6.73	53.16	216.58	134.58	26.94	20.63	0.49	—	1128.75	60.56	1025.98	HCO3-Na•Ca
S4	45.00	7.33	11.24	458.28	46.56	4.08	48.50	51.98	—	1099.39	61.20	1176.85	HCO3-Na
S5	73.50	8.21	7.79	112.90	8.92	0.84	14.84	29.34	25.90	198.88	48.06	315.32	HCO3-Na
S6	58.60	7.32	23.90	448.19	47.19	22.83	98.60	32.35	141.09	972.92	79.40	1313.54	HCO3-Na
S7	57.60	7.25	20.40	284.82	35.67	2.77	27.97	50.18	—	799.68	95.54	833.20	HCO3-Na



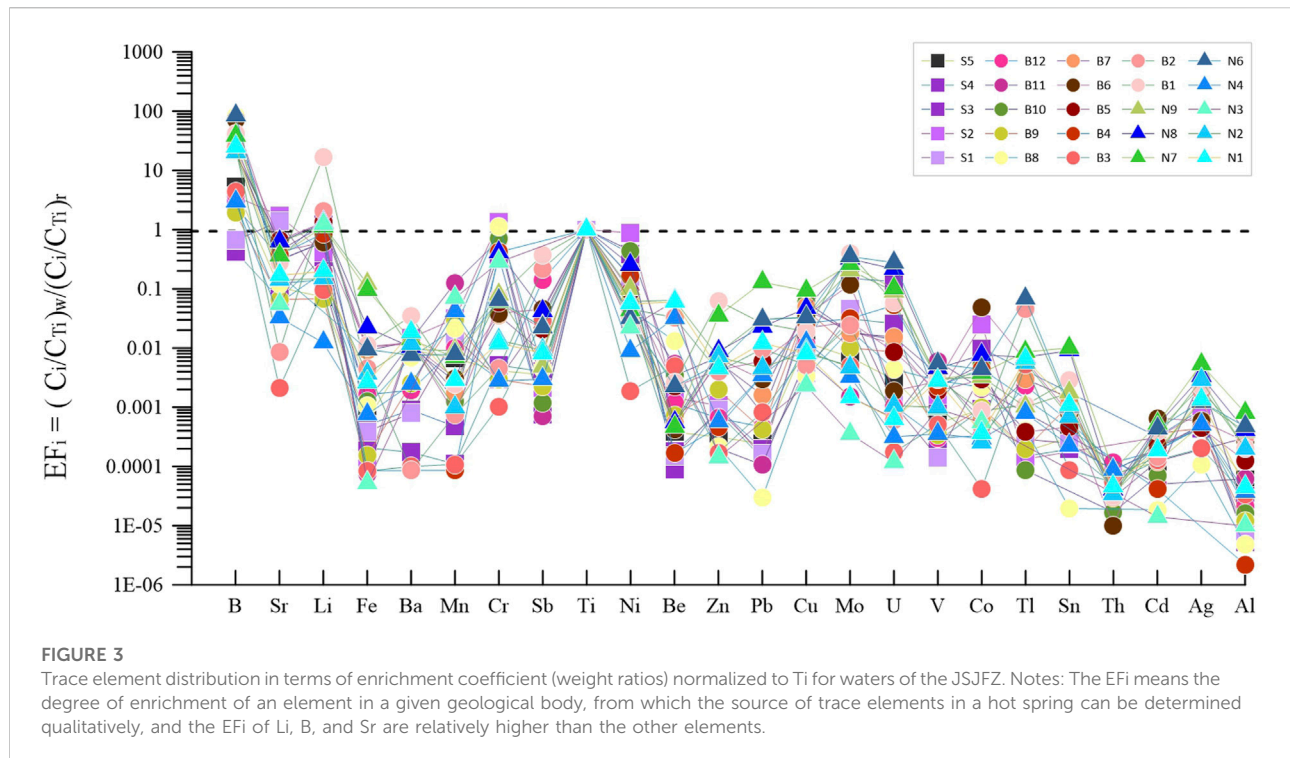
with a total length of 1,200 km and a width of 50–70 km (Xia and Zhu, 2020). In particular, its major faults cut deeply into the crust and even through the asthenosphere. Tectonically, the JSJFZ is cut into two segments by the NNE Batang fault (BTF) (Figure 1B), namely the Northern Jingshajiing fault (NJSJF) and the Southern Jinshajiing fault (SJSJF). The BTF is a dextral fault that strikes N30°E and dips to the northwest at a sharp angle, with a total length of about 200 km. High-temperature hot springs are distributed along the JSJF and BTF. Particularly, hot springs with temperature higher than 80°C have been found in the Batang geothermal field.

The area is covered by widespread Triassic limestone with multi-stage magmatic activity. It owns a well-developed fracture system and frequent earthquakes. Since 780 B.C., two large earthquakes with

magnitude >7.0 have occurred in this region, and minor to intermediate seismic events are frequent (Figure 1B). For the SJSJF, the dextral strike-slip rate is 4.9 mma^{-1} during the last 20 years, with a locking depth of approximately 20 km, while the slip rate of the NJSJF is not significant (Xu et al., 2020). For the BTF, the dextral strike-slip rate was $10.8 \pm 2.3 \text{ mma}^{-1}$ during 1999–2007 (Li et al., 2014), and its slip rate is consistent with that of the SJSJF in recent years (Xu et al., 2020).

3 Sampling and analysis

A total of 28 hot spring water samples were collected from the JSJFZ in 2018–2019. Based on the geological structure, the 28 hot



springs were divided into three sections: N1-N9 in the NJSJF, B1-B12 in the BTF and S1-S7 in the SJSJF, respectively. Among them, hot springs N3, N7, and N9 were located in the secondary fault of NJSJF (Figure 1B). The main sampling information is listed in Table 1.

All water samples were collected in new, colorless, polyethylene terephthalate (PET) bottles that had been rinsed with the water samples. Specific conductivity, pH, dissolved oxygen and temperature of the spring water samples were measured *in situ* by placing multi-parameter probes into the spring vents. Reagent-quality HNO₃ was added to each sample to lower down the pH below 1. The concentrations of cations and anions were measured by a Dionex ICS-900 ion chromatograph and an AS40 automatic sampler at the Earthquake Forecasting Key Lab of China Earthquake Administration (<https://www.ief.ac.cn/sysbygypt/>), with the reproducibility within ±2% and detection limits 0.01 mg/L. For SiO₂ analysis, the geothermal water samples were diluted ten-fold using deionized water to prevent precipitation of SiO₂ in water. Trace elements were analyzed at the Test Center of the Research Institute of Uranium Geology (<http://www.albriug.cn/>) by Element XR ICP-MS (Thermo Fisher, Bremen, Germany). The hydrogen and oxygen isotopes were measured using a Finnigan MAT253 mass spectrometer, *via* the TC/EA method. Results were expressed as parts per thousand deviations from the Vienna Standard Mean Ocean Water (V-SMOW). Precisions of ±0.2% (2S.D.) and ±1% (2S.D.) were obtained for δ¹⁸O and δD in a standard water sample, respectively (Wang et al., 2010).

4 Results and discussion

4.1 General hydrochemistry and origin of major ions

The 28 geothermal water samples in the study area were mainly divided into three categories, N1-N9, B1-B12, and S1-S7, respectively (Table 2). The Piper diagram in Figure 2 shows the distribution of the main cations (Ca²⁺, Mg²⁺, Na⁺, K⁺) and anions (HCO₃⁻, Cl⁻ and SO₄²⁻) of all water samples, which can be used to classify the hydrochemical characteristics of the water samples. It shows that Ca²⁺, Na⁺, and HCO₃⁻ are the main chemical components for most of the samples.

4.1.1 Hot springs from the NJSJF (N1-N9)

N1 - N9 are located in the major and secondary faults of the NJSJF. All these samples can be divided into two groups, N1, N2, N4, N5, N6, N8 in the major fault and N3', N7', N9' in the secondary fault of the NJSJF. Except for N2 (Ca-SO₄•HCO₃) and N7' (Na-Cl), the hydrochemical types of these hot spring water samples are Na-HCO₃ and Ca•Na-HCO₃ in the major and secondary faults of NJSJF. The temperatures of these hot springs are in the range of 10.57°C to 73.8°C, and the pH values vary between 6.57 and 8.25. Most of the spring water samples have low total dissolved solids (TDS) values ranging from 254.83 mg/L to 1757.77 mg/L, except for N7', which has a TDS value of 43,542.98 mg/L.

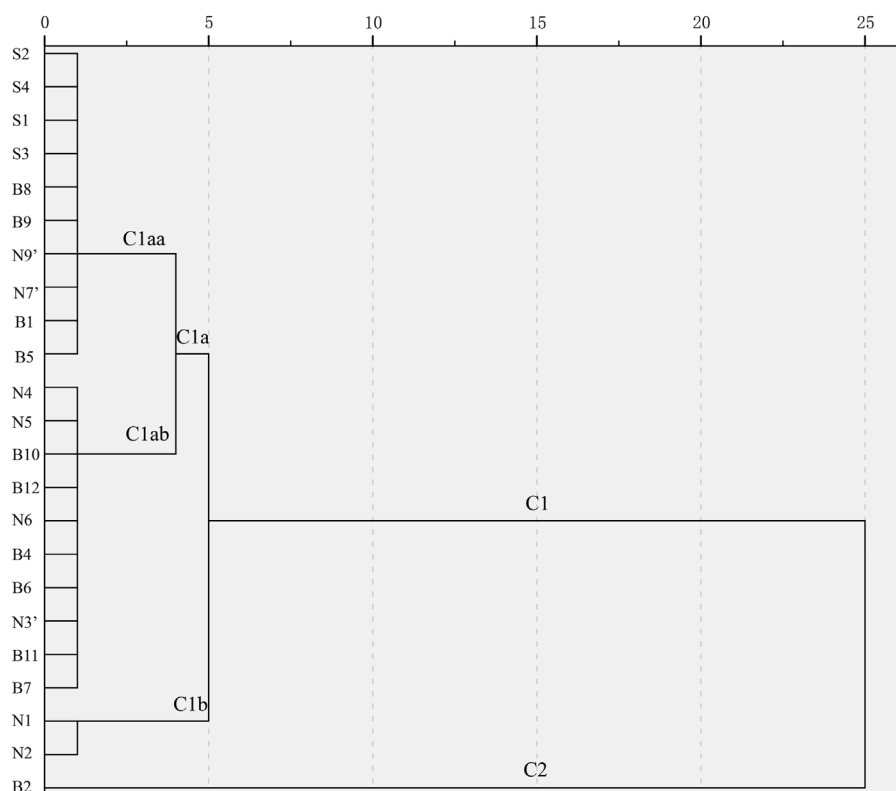


FIGURE 4

Cluster analysis of major ions of the spring water samples. Notes: All the samples can be divided into two parts, namely C1 and C2. And for C1, it can be divided into C1a and C1b. And furthermore, the C1a can be divided into C1aa and C1ab.

In the major fault of the NJSJF, as shown in Figure 2 (blue dots), most of hot spring water samples are distributed in “Zone 1”, where the hardness of carbonic acid exceeds 50% and the chemical properties of groundwater are mainly alkaline earth metals and weak acids. Their aquifers are located in the Triassic limestone. As for sample N5, it locates in “Zone 6”, where the carbonic alkali metal proportion is more than 50%. Na^+ in the spring water is mainly from the alternating dissolution and cation adsorption of albite, potassium feldspar, anorthite and other minerals. HCO_3^- mainly come from the dissolution of carbonate rocks such as limestone and dolomite (Yi et al., 2021). As for sample N2, it locates in “Zone 5”, where non-carbonic acid hardness exceeds 50%. Generally, as the depth of groundwater infiltration depth increases, the leaching effect is enhanced and the concentration of SO_4^{2-} in the spring water increases. Sample N2 is located in Triassic sandstone, mudstone, volcanic strata and limestone. Oxidation of pyrite in aqueous medium can accelerate the dissolution of limestone, so as to enrich the SO_4^{2-} in spring water.

In the secondary fault of the NJSJF, as shown in Figure 2 (green dots), the concentrations of Cl^- (25,238.17 mg/L), SO_4^{2-} (3708.77 mg/L), Na^+ (12,979.57 mg/L) and Ca^{2+} (1258.70 mg/L) in N7' are much higher than those in N3', N9'. The TDS value of N7' (43,542.98 mg/

L) is the highest one among the samples in the NJSJF. And N7' is located near the top of the right side of “Zone 2”, where non-carbonated alkali metal content is more than 50% and the groundwater chemistry is mainly alkali metal and strong acid. It may have originated from ancient seawater. During the water cycle, it was concentrated and finally became a deep brine with high salinity (Yan et al., 2021). Meanwhile, N9' is located in “Zone 6”, where the proportion of carbonic alkali metals exceeds 50%. Their origin is similar to that of N5.

4.1.2 Hot springs from the BTF (B1-B12)

B1–B12 are located in the BTF (Figure 2, red dots). The hydro-chemical types of these hot spring water samples are mainly Na-HCO_3 , $\text{Ca}\bullet\text{Na-HCO}_3$ and $\text{Na}\bullet\text{Ca-HCO}_3$. The temperature of these hot springs varies between 31.50°C and 86.1°C, and the pH value varies between 7.12 and 8.89. The TDS values of these spring water samples are relatively low, ranging from 378.96 mg/L ~ 1254.35 mg/L. Compared to the samples collected in the NSJSF, the hydro-chemical types of hot spring water samples in the BTF do not change significantly, i.e., Na-HCO_3 , $\text{Ca}\bullet\text{Na-HCO}_3$ and $\text{Na}\bullet\text{Ca-HCO}_3$. Only the hydro-chemical type of B9 is $\text{Ca}\bullet\text{Mg-HCO}_3$. The Na-HCO_3 type waters are located in “Zone 6”, while other samples are mainly located

TABLE 3 Hydrogen, oxygen and strontium isotopic compositions of the geothermal water samples.

Segment	$\delta^2\text{H}$ (‰)	$\delta^{18}\text{O}$ (‰)	$^{87}\text{Sr}/^{86}\text{Sr}$	Segment	Altitude (m)
N1	-131.50	-17.20	0.7134	N1	3,285
N2	-135.70	-17.90	0.7078	N2	3,994
N3'	-122.20	-14.90		N3	4,107
N4	-135.50	-17.40	0.7079	N4	2,906
N5	-148.20	-19.70	0.7142	N5	2,945
N6	-130.00	-17.20	0.7095	N6	2,964
N7'	-116.90	-15.40		N7	3,802
N8	-141.40	-18.10	0.7102	N8	3,313
N9'	-150.3	-20.2	0.7152	N9	3,952
B1	-151.20	-20.00	0.7124	B1	3,562
B2	-143.00	-24.20		B2	3,562
B3	-147.50	-20.00	0.7126	B3	3,287
B4	-158.20	-20.60	0.7158	B4	3,933
B5	—	—		B5	3,167
B6	-121.30	-15.30		B6	2,726
B7	-133.90	-17.50		B7	3,952
B8	-147.80	-19.50	0.7234	B8	2,668
B9	—	—		B9	2,517
B10	-144.70	-18.70	0.7206	B10	3,079
B11	-122.80	-15.40		B11	2,519
B12	-147.10	-18.90	0.7162	B12	2,513
S1	-148.60	-20.50		S1	2,646
S3	-158.70	-20.70	0.7208	S3	3,247
S4	-157.80	-20.80	0.7173	S4	3,099
S5	-143.80	-18.30		S5	2,655
S6	-145.60	-18.10		S6	3,270
S7	-144.60	-19.20		S7	3,235

in the transition region of “Zone 1” and “Zone 4”. It indicates that their source rocks are mainly limestone, dolomite, calcareous sandstone and siltstone.

4.1.3 Hot springs from the SJSJF (S1-S7)

S1–S7 are located in the SJSJF (Figure 2, purple dots). The hydro-chemical types of these hot spring water samples are mainly Na-HCO_3 and $\text{Ca}\bullet\text{Na-HCO}_3$. The temperature of these hot springs varies between 17.60°C and 73.50°C, and the pH value varies between 6.73 and 8.21. The TDS values of these spring water samples are relatively low, ranging from 315.32 mg/L~1313.54 mg/L. Minimal change of the hydro-chemical types of hot spring water samples is found in the SJSJF. All these spring waters are located in “Zone 6”, which is the same with some of the samples in the BTF. It indicates that their source rocks are much more similar, mainly limestone, dolomite.

To sum up, all these spring water samples in the JSJFZ have the following characteristics. Congruent and incongruent dissolution of aquifer rocks, hydrothermal conditions, hydrodynamic power, together with cation exchange reactions may strongly influence

the ionic concentration and facies types of the groundwater in the aquifer along the JSJFZ. Carbonate rocks are mainly developed in the study area, and HCO_3^- in the hot springs mainly comes from carbonate rocks, while Ca^{2+} and Mg^{2+} mainly come from soluble limestone (CaCO_3) and dolomite (MgCO_3) dissolved in the groundwater. In addition to dolomites, limestone, and carbonate rocks, sandstones and conglomerates are also developed in the study area, mainly including quartz, mica, feldspar and other aluminosilicate minerals, etc. Under high temperature and pressure, the recycled water reacts with aluminosilicate and carbonate rocks, causing a large amount of Na^+ , silicic acid, and carbonate in the surrounding rocks to dissolve in water (Zhang et al., 2003).

4.2 Origin of trace elements hot spring waters

Water-rock reactions during the deep groundwater circulation are responsible for the variation in trace element

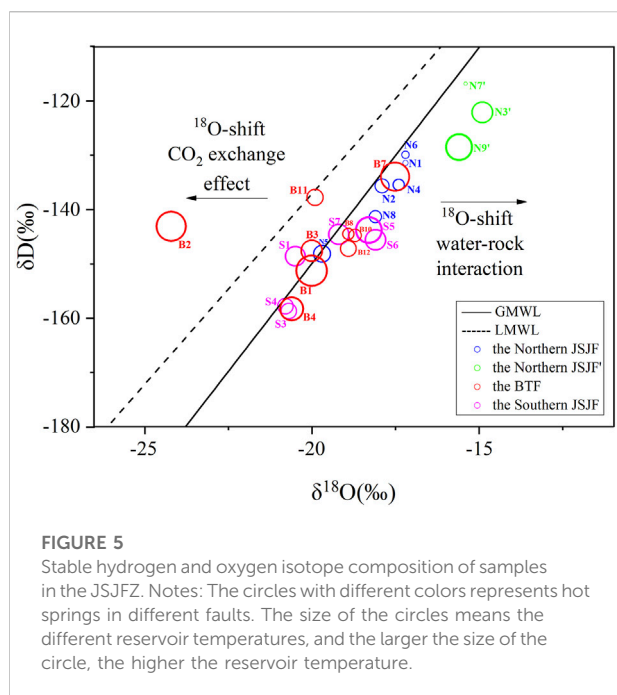


FIGURE 5

Stable hydrogen and oxygen isotope composition of samples in the JSJFZ. Notes: The circles with different colors represents hot springs in different faults. The size of the circles means the different reservoir temperatures, and the larger the size of the circle, the higher the reservoir temperature.

content. Therefore, the degree of water-rock reaction can be inferred to some extent by analyzing the trace element content characteristics. In this study, the trace elements measurements of 26 samples in the JSJFZ are shown in [Supplementary Table S1](#). Twenty-four kinds of trace elements were determined, including Ti, V, Cr, Fe, Co, Ni, Cu, Zn, Ag, Cd, Sn, Sb, Pb, Li, Be, B, Al, Sr, Mo, Ba, Tl, Th, U, and Mn. The enrichment factor (EF_i) is the degree of enrichment of an element in a given geological body, from which the source of trace elements in a hot spring can be determined qualitatively (Ji et al., 2017). The EF_i is calculated as follows:

$$EF_i = (C_i/C_R)_W / (C_i/C_R)_R \quad (1)$$

Where C_R is the selected reference elemental content, C_i is the elemental content in the sample, w and r is the elemental content in the water sample and the rock, respectively. Titanium (Ti) was chosen as the reference element, and the average content of trace elements in typical granites was used as the reference values from Ji et al. (2017).

As shown in [Figure 3](#), the EF_i of Li, B and Sr are relatively higher than the other elements. The mobile chalcophile elements may originate from external sources, such as sulfide-rich altered rocks. The content of alkali metal elements such as Li is generally lower than the major elements, but due to their active chemical properties, strong mobility, they are mainly enriched in acidic rocks with strong migration ability, and the content of some springs is close to or even exceeds the abundance of the surrounding rocks. The activity of Li may be a signature of deep fluid upwelling during deep fracture activity. Li-silicate minerals, such as lithium mica and chert, are usually formed

in volcanic and magmatic rocks, and Li can enter water in a dissolved state under hydrolysis (Zhang et al., 2003). However, the Li concentration in the hot springs of the JSJFZ is not as high as that in the Kangding area, indicating a lack of magmatic source in the JSJFZ (Yi et al., 2021).

Studies have shown that the deeper the groundwater cycle, the higher the B content, because the solubility of B in groundwater increases with depth and pressure (Cai et al., 2001; Zhang et al., 2003). Hot springs with high B content are mainly located in the middle segment of the JSJFZ, i.e. the BTF, indicating that the circulation depth of hot springs in the BTF is larger.

Alkaline-earth metal Sr is a disperse element with high abundance in the crust, mantle and weak alkaline water with a pH of 7.0–8.5 (Cai et al., 2001). In addition, Sr is usually associated with calcium and potassium and is therefore present in calcium and potassium-rich minerals such as potassium feldspar and hornblende (Zhang et al., 2003). Volcanic and granitic rocks rich in potassium feldspar and hornblende are developed in this study area. The pH value of spring water samples in the JSJFZ ranged from 6.57 to 8.89 with a mean value of 7.53, which was favorable for Sr enrichment. Groundwater is heated and reacted at fracture depths, and is recycled into hot spring water after a series of reactions.

The cluster analysis of the major ions in the water samples from the JSJFZ shows that sample B2 in the BTF is different from the other samples ([Figure 4](#)) when the center distance is set as 10. Combined with the δD and $\delta^{18}O$ values of sample B2 ([Table 3](#); [Figure 5](#)), it indicates that the water-rock reaction here is stronger than elsewhere.

4.3 Origin of hot spring waters

Stable oxygen and hydrogen isotopes have been widely used to determine the source, transit time of geothermal fluids (Tian et al., 2018). Therefore, the relationship between δD and $\delta^{18}O$ of water samples was plotted to trace the source of replenishment of geothermal fluids. In the study area, the δD and $\delta^{18}O$ values of geothermal water samples ([Table 3](#)) ranged from -158.7‰ to -116.9‰ and -24.2‰ to -14.9‰ (VSMOW). As shown in [Figure 5](#), the majority of the geothermal waters is plotted close to the Global Meteoric Water Line (Craig, 1961) and the western Sichuan Meteoric Water Line (Chen et al., 2014), indicating the recharge source of meteoric water. An exception is the spring water sample (B2) in the BTF, which may be attributable to the isotopic exchange reaction between water and CO_2 isotopes (Pang et al., 2017). Groundwater is induced by precipitation recharging from high altitude regions. Aquifer rocks dissolved in the infiltrating water and freshening started, consisting of cation exchange during groundwater flow. δD and $\delta^{18}O$ values are more negative for springs at high mountains or high latitudes, and less negative for springs at low altitudes and low latitudes.

Sr concentration and $^{87/86}Sr$ values varied from 0.03 to 13.51 $\mu\text{g/L}$ and 0.7078 to 0.7234, respectively. The spring

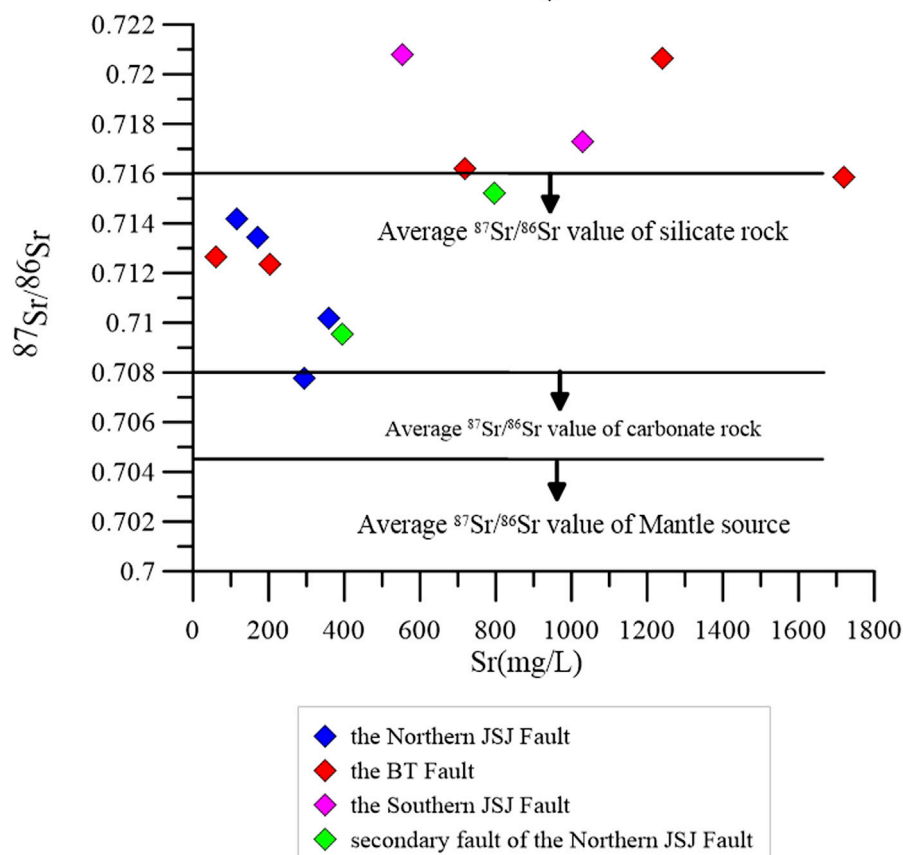


FIGURE 6
Strontium isotopes of the water samples in the JSJFZ.

waters in the NJSJF had lower Sr concentrations than those in the NJSJF and BTF. The $^{87}\text{Sr}/^{86}\text{Sr}$ values of the spring waters in the NJSJF were closer to the average $^{87}\text{Sr}/^{86}\text{Sr}$ value of carbonate rock (Figure 6), while the $^{87}\text{Sr}/^{86}\text{Sr}$ values of the spring waters in the BTF and the SJSJF belonged to the aluminosilicate weathering. The segmental characteristics of the different strontium isotopes suggest that the hot springs were formed by the interaction with Sr-bearing source rocks in the crust during the deep circulation of atmospheric precipitation in the local heat flow system. This is consistent with the geochemical characteristics of the hot spring waters and the lithology of the surrounding rocks.

4.4 Water-rock interaction of hot springs in the JSJFZ

4.4.1 The water-rock reaction equilibrium

The Na-K-Mg ternary diagram (Figure 7) can indicate the degree of ionic equilibrium reaction of the water sample. As shown in Figure 7, the blue and green circles represent water

samples in the NJSJF. Except for sample N7', the other samples are distributed in the "immature waters zone". The red circles represent the water samples in the BTF, which are distributed in the "immature waters zone" or the "partially equilibrated and mixed waters zone." And the purple circles represent water samples in the SJSJF that are distributed in the "immature waters zone" or the "partially equilibrated and mixed waters zone". It can be preliminarily estimated that the spring waters in the BTF have the highest reservoir temperatures in the JSJFZ.

4.4.2 Mineral saturation states

Mineral equilibrium calculations help predict the presence of reactive minerals and estimate mineral reactivity in groundwater systems. By using the saturation index (SI) approach, reactive minerals in host rocks and minerals that may precipitate during the extraction and use of thermal fluids can be predicted from groundwater data without the need to examine solid phases samples (Deutsch, 1997). The mineral saturation indices of hydrothermal minerals that may be present in the reservoirs of geothermal systems

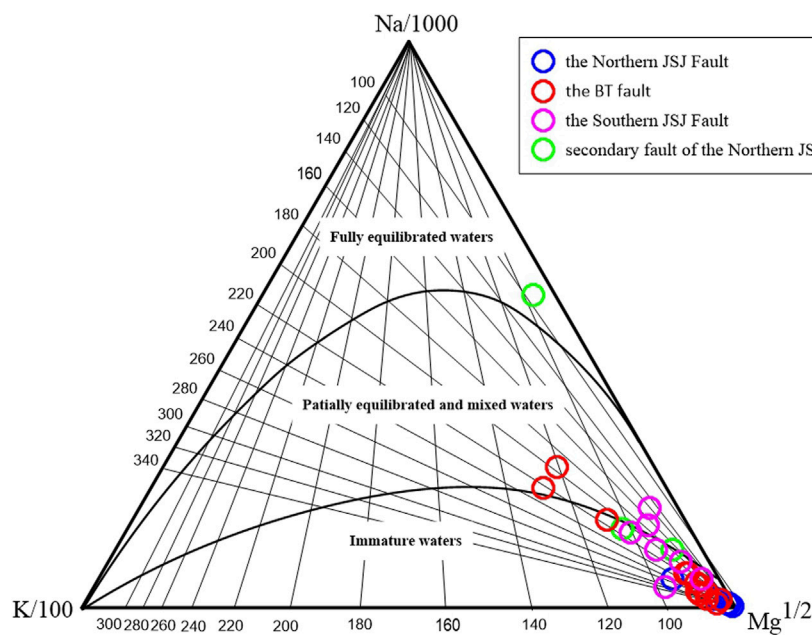


FIGURE 7
Distribution of aqueous samples on the Na-K-Mg ternary diagram.

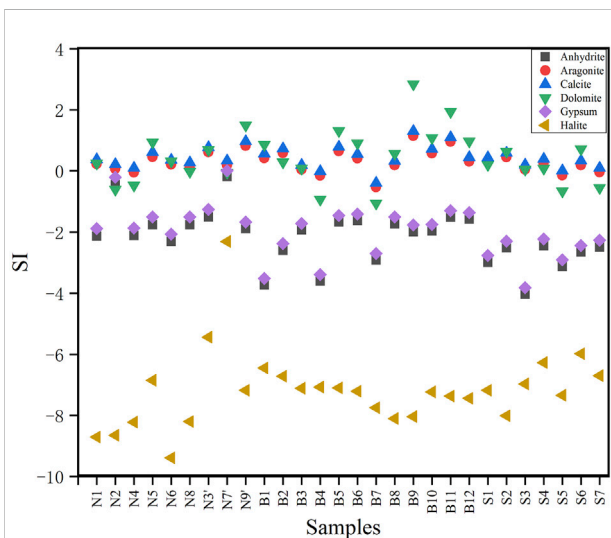


FIGURE 8
Saturation indices values of water samples with respect to minerals. Notes: The value of SI is divided by zero.

were calculated by PHREEQCI-2.12 (USGS) at their outlet temperatures and pH values. Results are presented in Figure 8. Almost all groundwater samples were supersaturated (SI > 0) relative to calcite at the sampling temperature, suggesting that CO₂ degassing may have occurred (Figure 8). Only the value of sample B7 was negative (−0.39), but it was also almost in equilibrium

with calcite. This super-saturation state demonstrates the presence of substantial amounts of these minerals and sufficient residence time in the aquifer system (Rouabhia et al., 2012). Except for B4 and B7, groundwater samples were in equilibrium with dolomite (SI=0). The possible cause of B4 and B7's characteristics is that high CO₂ concentrations lead to lower pH values and lower dolomite SI values (Zhou et al., 2020a). Almost all groundwater samples are in under saturation with halite (SI <−4). The rest of minerals in Supplementary Table S2 have various saturation indices.

4.4.3 Reservoir temperature and circulation depth

Chemical geothermometers (including quartz and chalcedony) and cationic geothermometers (including Na-K and Na-Li system) are commonly used to estimate reservoir temperatures. The equations are as follows:

$$T_{\text{SiO}_2} (\text{ }^\circ\text{C}) = (1309 / (5.19 - \log(\text{SiO}_2))) - 273.15 \text{ (Fournier, 1981)} \tag{2}$$

$$T_{\text{Na-K}} (\text{ }^\circ\text{C}) = (1217 / (1.483 + \log(\text{Na}/\text{K}))) - 273.15 \text{ (Fournier, 1981)} \tag{3}$$

$$T_{\text{Na-K}} (\text{ }^\circ\text{C}) = (1390 / (1.75 + \log(\text{Na}/\text{K}))) - 273.15 \text{ (Giggenbach, 1988)} \tag{4}$$

$$T_{\text{Na-Li}} (\text{ }^\circ\text{C}) = (1590 / (0.779 + \log(\text{Na}/\text{Li}))) - 273.15 \text{ (Kharaka and Mariner, 1984)} \tag{5}$$

These geothermometers consist of equations or models based on temperature-dependent chemical reactions, from

TABLE 4 Calculation of reservoir temperature and circulation depth of geothermal waters.

Sample no.	T _{outlet} (°C)	T _{Na-K} (°C)	T _{Na-K} (°C)	T _{Na-Li} (°C)	T _{SiO2} (°C)	T _{Silicon enthalpy mixing model} (°C)	T _{optimum} (°C)	Proportion of cold water (%)	D _{SiO2} (km)	D _{S-E} (km)
	Fournier, 1981		Arnorsson, 1998		Kharaka and Mariner, 1984		Fournier, 1981		Fournier and Truesdell, 1974	
N1	16	227	242	—	60	—	60	—	0.9	—
N2	41	177	195	163	96	103	96	71	1.7	1.8
N3	59	192	209	230	117	85	117	34	2.1	1.5
N4	33	212	228	150	75	73	75	71	1.3	1.2
N5	49	248	261	160	102	102	102	62	1.8	1.8
N6	23	234	249	—	45	—	45	—	0.6	—
N7	11	55	77	21	36	—	36	—	0.4	—
N8	35	248	262	190	80	84	80	72	1.4	1.4
N9	73	157	176	165	133	125	133	48	2.5	2.3
B2	86	210	226	295	215	272	215	73	4.2	5.4
B3	66	190	208	204	140	153	140	63	2.6	2.9
B4	66	199	216	233	131	134	131	58	2.4	2.5
B6	53	203	220	159	124	149	124	72	2.3	2.8
B7	80	196	214	240	156	157	156	55	2.9	3.0
B8	35	233	248	204	93	136	93	85	1.6	2.5
B10	35	226	241	239	97	146	97	86	1.7	2.7
B11	46	272	284	225	104	115	104	70	1.9	2.1
B12	48	287	297	235	128	172	128	80	2.4	3.3
S3	45	307	315	187	111	140	111	77	2.0	2.6
S4	45	119	140	172	111	142	111	77	2.0	2.7
S5	74	186	204	190	100	—	100	—	1.8	—
S6	59	167	186	246	124	135	124	64	2.3	2.5
S7	58	189	207	226	134	158	134	71	2.5	3.0

T_{outlet} means the outlet temperature of hot spring; T_{Na-K}, T_{Na-Li} and T_{SiO2} means reservoir temperature calculated by different geothermometers; T_{optimum} means the most appropriate reservoir temperature; D_{SiO2} and D_{S-E} means the depths calculated by SiO₂ geothermometers and silicon enthalpy mixing model, respectively.

which equilibrium temperatures can be calculated. In fact, due to the complex geological settings, different chemical geothermometers always yield very different reservoir temperatures. In this study, we compared these calculation results (Table 4). The Na-K-Mg triangle diagram method could help to judge the equilibrium state of the geothermal water (Giggenbach, 1988). In Figure 7, the spring water samples are almost belong to immature waters, indicating that they are not fully equilibrated with the reservoir rocks, so the cation ratio geothermometers cannot provide reliable results than silica geothermometer with no-steam loss. Finally, we chose the quartz geothermometers with no steam loss (Fournier, 1981) as the optimum one. The circulation depth of the spring waters and the proportion of cold water were also deduced using the reservoir temperatures calculated by the Silicon-enthalpy mixing model (Fournier and Truesdell, 1974). The results showed that the T_{SiO2} of the

NJSJF, BTF and SJSJF ranged from 36 to 133°C, 93 to 215°C and 100 to 134°C, respectively; the T_{S-E} of the NJSJF, BTF and SJSJF ranged from 73 to 125°C, 115 to 272°C and 135 to 158°C, respectively. The results are close to those of Tian et al. (2019) on the BTF hot springs. The spatial distribution of outlet temperature and thermal reservoir temperature was consistent with each other. The spring water temperature in the southern segment of the JSJFZ was higher than that of the northern segment, with the peak located in the BTF.

The circulation depths were evaluated according to the following equation:

$$D(\text{km}) = ((T - T_0)/\Delta t) + h \quad (7)$$

D is the circulation depth; T is the reservoir temperature (°C); T₀ is the temperature of the local average temperature (°C); Δt is the geothermal gradient (°C/km) and h is the depth of

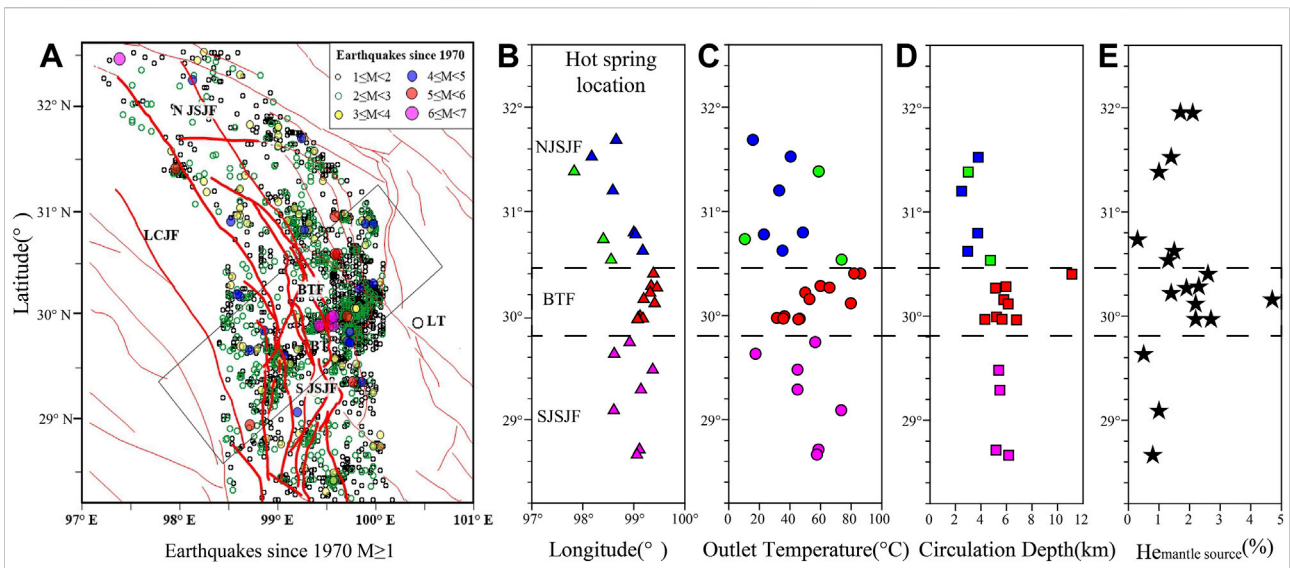


FIGURE 9 Earthquake ($M \geq 1$) distribution in the JSJFZ since 1970 (A), hot spring location (B), outlet temperature (C), circulation depth (D) and mantle source helium (E), data from Zhou et al., 2020a).

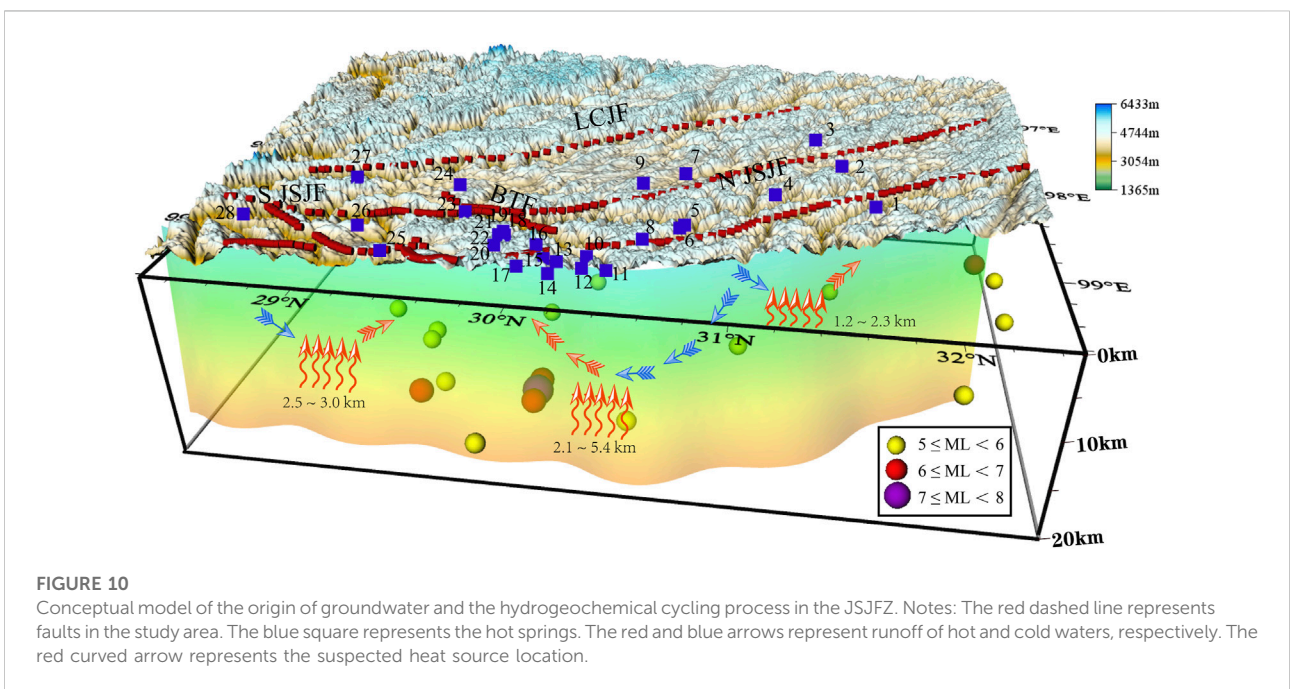


FIGURE 10 Conceptual model of the origin of groundwater and the hydrogeochemical cycling process in the JSJFZ. Notes: The red dashed line represents faults in the study area. The blue square represents the hot springs. The red and blue arrows represent runoff of hot and cold waters, respectively. The red curved arrow represents the suspected heat source location.

constant temperature zone (km). For the Sichuan province, Δt , T_0 , h was assumed as 47.5°C/km, 16.42°C and 0.02km, respectively (Zhang et al., 2019).

The D_{SiO_2} of the NJSJF, BTF and SJSJF was 0.4–2.5 km, 1.6–4.2 km and 1.8–2.3 km, respectively. And the D_{S-E} of the NJSJF, BTF and SJSJF was 1.2–2.3 km, 2.1–5.4 km and 2.5–3.0 km. Similarly, the circulation depth of the spring waters in the BTF was the deepest.

4.5 Correlation between hydro-geochemical changes and seismic activities

4.5.1 Segmental hydro-chemical characteristics and spatial distribution of earthquakes

Generally, the ranking of the JSJFZ spring waters in terms of temperature, thermal reservoir temperature, circulation depth,

water maturity, water-rock interaction intensity is roughly $NJSJF < SJSJF < BTF$. For historical earthquakes ($M \geq 5$) in the JSJFZ (Figure 1), they used to appear in the NJSJF and BTF, and for recent earthquakes ($M \geq 1$) in the JSJFZ, they gathered in the BTF (Figure 9A). It may be due to two mechanisms. The spring waters in the BTF contain more mantle derived materials (Zhou et al., 2017; Zhou et al., 2020a), which confirms that the BTF is characterized by a deep and large fault cutting through the crust or an ultra-crustal fault. Given its strong fault activity, the BTF became an earthquake-prone area. As shown in Figures 9B–E, the outlet temperature, circulation depth and mantle source helium in the hot springs of the BTF were the highest in the JSJFZ. Deep fluid circulation and fracture coupling are important triggers of earthquakes. It can be inferred that the first mechanism is more consistent with the characteristics of the JSJFZ. In addition, the effects between fluids and earthquakes are mutual. On the one hand, deep-source fluids promote the occurrence of earthquakes, and on the other hand, the occurrence of earthquakes changes the crustal structure and fluid permeability (Manga and Wang, 2015).

Strong earthquakes may occur in the transition zone of geothermal anomalies (Liu et al., 2022). According to spatial distribution of the reservoir temperatures in the JSJFZ, the BTF coincides with the high and low temperature transition zone where the north-south segment intersects. Earthquakes are more expected to occur in the BTF rather than other areas due to its strong fluid activity characteristics and deep cutting depth. In fact, the BTF has been active since the late Quaternary. In 1870, the Batang M seven earthquake occurred here. According to the GPS measurements, the BTF has a dextral strike slip rate of 8.7 ± 2.1 mm/a (Wang et al., 2008). In the NJSJF, the fault slip is not significant, while in the BTF and the SJSJF, the slip rate reached ~ 4.9 mm/a (Xu et al., 2020). Correspondingly, the hot springs in the BTF were the most active, and a large number of earthquakes also gathered here. In the BTF and SJSJF area, the locking depth is about 20 km (Xu et al., 2020) and there is a certain degree of strain accumulation in the faults. Earthquakes usually occur on faults with accumulated stresses, especially in areas with strong and weak stress transitions. Based on fracture activity, seismic distribution and geochemical characteristics of the hot springs, the BTF is currently at higher seismic risk than other areas in the JSJFZ.

4.5.2 Conceptual model and evolution of geothermal fluid in JSJFZ

Deep fracture zones can serve not only as a channel for further infiltration of groundwater, but also as a channel for rapid ascent of deep-derived geothermal fluid. It is noted that deep source fluids can trigger earthquakes (Fairley et al., 2003; Shi and wang, 2017; Hou et al., 2018; Wang et al., 2021). When a large amount of fluid invades into a fault, it may change the pore pressure and the stress state in the fault zone. Therefore, it may increase the frequency of minor and intermediate earthquakes. Besides, heat sources, permeability

pathways and fault activity also play important roles in formation of hot springs (Chen et al., 2014; Zhou et al., 2020b). Tracing the sources and migration pathways of groundwater in active fault zones is of paramount importance in terms of studying hydro-geochemical precursors in seismic hazards zones.

A conceptual model for the origin of groundwater and the hydro-geochemical cycling process in the JSJFZ is summarized in Figure 10 according to the results of this study. Meteoric waters permeates into the aquifers along the fractures between and around mountains and river terraces through the water-conducting fault zone. Due to the difference in circulation depth, reservoir temperature and degree of water-rock reaction, partially equilibrated water or immature water were formed in the NJSJF, the BTF and the SJSJF. The spring water may mix with cold surface water or shallow groundwater with different mixing ratios during fluid ascent in the fault channel. Finally, it became exposed to the earth's surface as a hot spring. When the crustal stress in the JSJFZ changes, the pressure in the aquifer system and the equilibrated state of hot spring water will be disrupted, resulting in the different hydro-chemical characteristics. The infiltrated waters in the BTF had a considerable deep circulation (~ 5.4 km) in a high heat flow reservoir. This is the reason for the high mantle helium contribution (Tian et al., 2018; Zhou et al., 2020a), and the frequent high-intensity earthquakes here. Deeply-sourced volatile emissions may have responded rapidly to the onset of sustained plateau growth (Zhang et al., 2021).

The Rayleigh-wave velocity of the NJSJF is higher than that of the southern SYDSB (Fan et al., 2015). The SJSJF is located in the low-velocity channel bounded by major strike-slip faults around the EHS and in the southeastern margin of Tibet (Bao et al., 2015; Hu et al., 2018). The high-resolution Q_{lg} model showed that the main flow channel emerged from the northern end of plateau, extended east and southeast, and then turned south after being blocked by the rigid Sichuan Basin (Zhao et al., 2013). Consistently, the conductance values present very high conductivity regions near the SJSJF. As the fluid content increases, the crust weakens and flows (Unsworth et al., 2005). And crustal flows can occur in orogenic belts and contribute to the uplift of plateau (Bai et al., 2011). High conductivity and low velocity layer is a relatively soft medium, which is prone to deformation, stress and strain conduction, concentration and accumulation. The BTF is located in the transition area of the NJSJF and SJSJF (Wang and Shen, 2020) that is prone to earthquakes. The geophysical and fluid geochemical signatures here are well confirmed by each other. In summary, the hydrological characteristics of hot spring water in fault zones play a crucial role in receiving information on tectonic movements and seismic activities in advance.

5 Conclusion

Fault structures and tectonic movements jointly control the formation and geochemical characteristics of hot springs. The

high-temperature geothermal system along the lithospheric-scale strike-slip JSJFZ was studied.

The geochemical characteristics of the 28 hot springs suggested that they were mainly recharged by atmospheric precipitation from the nearby mountains. Chemical geothermometry applications, together with silicon enthalpy mixing model calculation, presented a reservoir temperature range of 73 ~ 272°C. The proportion of cold water ranged from 34% to 86%. And the circulation depths varied from 1.2 km to 5.4 km.

A conceptual model for the hot spring water origin and circulation cycle showed that the meteoric water firstly seeped into the fault and was heated by the wall rocks. Then, it circulated along faults and fissures to the surface, where it eventually formed hot springs.

The segmental characteristics of the fault, the hydration characteristics together with the H, O, and Sr isotopes of the hot springs located in different segments of the JSJFZ and the seismic activities are closely related to each other. Notably, the hot springs in the BTF had deeper recharges source and high reservoir temperatures than those in the NJSJF and the SJSJF. And it was coincident with strong tectonic and seismological activity here in the BTF. Thus, the spatial distribution hot springs, the hydro-geochemical characteristics and the influence of controlling factors are of great importance to further exploration of strong seismic information.

Data availability statement

The original contributions presented in the study are included in the article/[Supplementary Material](#), further inquiries can be directed to the corresponding authors.

Author contributions

JL as the first author of this manuscript, wrote the main part of the article. XZ and YL as the corresponding authors, controlled the article ideas. MH, JL, JD, and FL helped collect the water samples. JT, YY, and SO made their contributions in the data analysis.

References

- Bai, D. H., Unsworth, M. J., Meju, M. A., Ma, X., Teng, J., Kong, X., et al. (2011). Crustal deformation of the eastern Tibetan plateau revealed by magnetotelluric imaging. *Nat. Geosci.* 497, 358–362. doi:10.1038/ngeo830
- Bao, X., Sun, X., Xu, M., Eaton, D. W., Song, X., Wang, L., et al. (2015). Two crustal low-velocity channels beneath SE Tibet revealed by joint inversion of Rayleigh wave dispersion and receiver functions. *Earth Planet. Sci. Lett.* 415, 16–24. doi:10.1016/j.epsl.2015.01.020
- Bo, Y., Liu, C., Zhao, Y., and Wang, L. (2015). Chemical and isotopic characteristics and origin of spring waters in the lanping-simao basin, yunnan, southwestern China. *Geochemistry* 75 (3), 287–300. doi:10.1016/j.chemer.2015.04.002

Funding

The work was funded by the Natural Science Foundation of Shaanxi Province, China (2022JQ-254), Spark Program of Earthquake Sciences (XH21032), National Key Research and Development Project (2017YFC1500501-05 and 2019YFC1509203), the National Natural Science Foundation of China (41673106, 42073063, and 4193000170), the Special Fund of the Institute of Earthquake Forecasting, China Earthquake Administration (2021IEF0101, 2021IEF0201, and 2021IEF1201) and Open Fund for Earthquake Forecasting (2021EFOF03).

Acknowledgments

We thank the Editor and two reviewers for their constructive comments and suggestions.

Conflict of interest

The authors declare that the research was conducted in the absence of any commercial or financial relationships that could be construed as a potential conflict of interest.

Publisher's note

All claims expressed in this article are solely those of the authors and do not necessarily represent those of their affiliated organizations, or those of the publisher, the editors and the reviewers. Any product that may be evaluated in this article, or claim that may be made by its manufacturer, is not guaranteed or endorsed by the publisher.

Supplementary Material

The Supplementary Material for this article can be found online at: <https://www.frontiersin.org/articles/10.3389/feart.2022.1015134/full#supplementary-material>

- Chen, Z., Du, J. G., Zhou, X. C., Yi, L., Liu, L., Xie, C., et al. (2014). Hydrochemistry of the hot springs in western sichuan province related to the WenchuanMS8.0 earthquake. *Sci. World J.* 2014, 1–13. doi:10.1155/2014/901432
- Craig, H. (1961). Isotopic variations in meteoric waters. *Science* 133 (3465), 1702–1703. doi:10.1126/science.133.3465.1702
- Deutsch, W. J. (1997). *Groundwater geochemistry: Fundamentals and applications to contamination*. New York, NY, USA: Lewis Publisher.
- Fairley, J., Heffner, J., and Hinds, J. (2003). Geostatistical evaluation of permeability in an active fault zone. *Geophys. Res. Lett.* 30 (18), 1962. doi:10.1029/2003gl018064

- Fan, L. P., Wu, J. P., and Fang, L. H. (2015). The characteristics of Rayleigh group velocities in the southeastern margin of the Tibetan Plateau and its tectonic implications. *Chin. J. Geophys.* 58 (5), 1555–1567. in Chinese. doi:10.6038/cjg20150509
- Fournier, R. O. (1981). "Application of water geochemistry to geothermal exploration and reservoir engineering," in *Geothermal systems, principles and case histories*. Editors L. Rybach and L. J. P. Muffler (New York: Wiley), 109–143.
- Fournier, R. O., and Truesdell, A. H. (1974). Geochemical indicators of subsurface temperature Part II, estimate of temperature and fractions of hot water mixed with cold water. *J. Res. U.S. Geol. Surv.* 2 (3), 263–270. doi:10.3133/ofr741032
- Fu, C. C., Lai, C. W., Yang, T. F., Hilton, D. R., Chen, C. H., Walia, V., et al. (2021). An automatic system for continuous monitoring and sampling of groundwater geochemistry in earthquake-prone regions of SW Taiwan. *Front. Earth Sci. (Lausanne)*. 9, 635913. doi:10.3389/feart.2021.635913
- Fulton, P. M., and Saffer, D. M. (2009). Potential role of mantle-derived fluids in weakening the San Andreas Fault. *J. Geophys. Res.* 114, B07408. doi:10.1029/2008JB006087
- Giggenbach, W. F. (1988). Geothermal solute equilibria. derivation of Na-K-Mg-Ca geothermometers. *Geochim. Cosmochim. Acta* 52, 2749–2765. doi:10.1016/0016-7037(88)90143-3
- Hou, Y. Y., Shi, Z. M., and Mu, W. Q. (2018). Fluid geochemistry of fault zone hydrothermal system in the yidun-litang area, eastern Tibetan Plateau geothermal belt. *Geofluids* 2018, 1–13. doi:10.1155/2018/6872563
- Hu, J. F., Badal, J., Yang, H. Y., Li, G., and Peng, H. (2018). Comprehensive crustal structure and seismological evidence for lower crustal flow in the southeastern margin of Tibet revealed by receiver functions. *Gondwana Res.* 55, 42–59. doi:10.1016/j.gr.2017.11.007
- Ji, L., Liu, F. L., and Wang, F. (2017). Multiple granitic magma events in north middle segment of Diancangshan Ailaoshan complex zone: Implications for tectonic evolution. *Acta Pet. Sin.* 33, 2957–2974. in Chinese.
- Jonsson, S., Segall, P., Pedersen, R., and Bjornsson, G. (2003). Post-earthquake ground movements correlated to pore-pressure transients. *Nature* 424, 179–183. doi:10.1038/nature01776
- King, C. Y. (1986). Gas geochemistry applied to earthquake prediction: An overview. *J. Geophys. Res.* 91 (B12), 12269–12281. doi:10.1029/jb091ib12p12269
- Kitagawa, Y., Koizumi, N., and Tsukuda, T. (1996). Comparison of postseismic groundwater temperature changes with earthquake-induced volumetric strain release: Yudani Hot Spring, Japan. *Geophys. Res. Lett.* 23 (22), 3147–3150. doi:10.1029/96GL02517
- Li, Y. H., Hao, M., Ji, L. Y., and Qin, S. L. (2014). Fault slip rate and seismic moment deficit on major active faults in mid and south part of the Eastern margin of Tibet plateau. *Chin. J. Geophys.* 57 (4), 1062–1078. in Chinese. doi:10.6038/cjg20140405
- Linde, A. T., Suyehiro, K., Miura, S., Sacks, I. S., and Takagi, A. (1988). Episodic aseismic earthquake precursors. *Nature* 334, 513–515. doi:10.1038/334513a0
- Liu, W., Guan, L. F., Liu, Y., Xie, X., Zhang, M., Chen, B., et al. (2022). Fluid geochemistry and geothermal anomaly along the yushu-ganzi-xianshuihe fault system, eastern Tibetan plateau: Implications for regional seismic activity. *J. Hydrol. X.* 607, 127554. doi:10.1016/j.jhydrol.2022.127554
- Manga, M., and Wang, C. Y. (2015). *Earthquake hydrology, treatise on geophysics*. Amsterdam: Elsevier.
- Martinelli, G., and Tamburello, G. (2020). Geological and geophysical factors constraining the occurrence of earthquake precursors in geofluids: A review and reinterpretation. *Front. Earth Sci.* 8, 596050. doi:10.3389/feart.2020.596050
- Nakagawa, K., Yu, Z. Q., Berndtson, R., and Hosono, T. (2020). Temporal characteristics of groundwater chemistry affected by the 2016 Kumamoto earthquake using selforganizing maps. *J. Hydrol. X.* 582, 124519. doi:10.1016/j.jhydrol.2019.124519
- Pang, Z. H., Kong, Y. L., Li, J., and Tian, J. (2017). An isotopic geoinicator in the hydrological cycle. *Procedia Earth Planet. Sci.* 17, 534–537. doi:10.1016/j.proeps.2016.12.135
- Rosen, M. R., Binda, G., Archer, C., Pozzi, A., Michetti, A. M., and Noble, P. J. (2018). Mechanisms of earthquake-induced chemical and fluid transport to carbonate groundwater springs after earthquakes. *Water Resour. Res.* 54, 5225–5244. doi:10.1029/2017wr022097
- Rouabhi, A., Djabri, L., Hadji, R., Baali, F., and FehdiHani, C. A. (2012). Geochemical characterization of groundwater from shallow aquifer surrounding Fetzara Lake NE Algeria. *Arab. J. Geosci.* 5, 1–13. doi:10.1007/s12517-010-0202-6
- Scholz, C. H., Sykes, L. R., and Aggarwal, Y. P. (1973). Earthquake prediction: A physical basis. *Science* 181, 803–810. doi:10.1126/science.181.4102.803
- Shi, Z. M., and Wang, G. C. (2017). Evaluation of the permeability properties of the Xiaojiang Fault Zone using hot springs and water wells. *Geophys. J. Int.* 209 (3), 1526–1533. doi:10.1093/gji/ggx113
- Skelton, A., Andren, M., Kristmannsdottir, H., Stockmann, G., Morth, C. M., Sveinbjornsdottir, A., et al. (2014). Changes in groundwater chemistry before two consecutive earthquakes in Iceland. *Nat. Geosci.* 7, 752–756. doi:10.1038/ngeo2250
- Tang, X. C., Zhang, J., Pang, Z. H., Hu, S., Wu, Y., and Bao, S. (2017). Distribution and Genesis of the eastern Tibetan Plateau geothermal belt, Western China. *Environ. Earth Sci.* 76 (1), 31. doi:10.1007/s12665-016-6342-6
- Thomas, D. (1988). Geochemical precursors to seismic activity. *Pure Appl. Geophys.* 126, 241–266. doi:10.1007/BF00878998
- Tian, J., Pang, Z. H., Guo, Q., Wang, Y., Li, J., Huang, T., et al. (2018). Geochemistry of geothermal fluids with implications on the sources of water and heat recharge to the Rekeng high-temperature geothermal system in the Eastern Himalayan Syntax. *Geothermics* 74, 92–105. doi:10.1016/j.geothermics.2018.02.006
- Tian, J., Pang, Z. H., Wang, Y. C., and Guo, Q. (2019). Fluid geochemistry of the Cuopu high temperature geothermal system in the eastern Himalayan syntaxis with implication on its Genesis. *Appl. Geochem.* 110, 104422. doi:10.1016/j.apgeochem.2019.104422
- Tian, J., Pang, Z., Liao, D. W., and Zhou, X. (2021). Fluid geochemistry and its implications on the role of deep faults in the Genesis of high temperature systems in the eastern edge of the Qinghai Tibet Plateau. *Appl. Geochem.* 131, 105036. doi:10.1016/j.apgeochem.2021.105036
- Unsworth, M. J., Jones, A. G., Wei, W., Marquis, G., Gokarn, S. G., and Spratt, J. E. (2005). Crustal rheology of the Himalaya and Southern Tibet inferred from magnetotelluric data. *Nature* 438 (7064), 78–81. doi:10.1038/nature04154
- Wang, B., Zhou, X. C., Zhou, Y. S., Yan, Y., Li, Y., Ouyang, S., et al. (2021). Hydrogeochemistry and precursory anomalies in thermal springs of Fujian (Southeastern China) associated with earthquakes in the Taiwan Strait. *Water* 13, 3523. doi:10.3390/w13243523
- Wang, C. Y., Cheng, L. H., Chin, C. V., and Yu, S. B. (2001). Coseismic hydrologic response of an alluvial fan to the 1999 Chi-Chi earthquake, Taiwan. *Geol.* 29 (9), 831–834. doi:10.1130/0091-7613(2001)029<0831:chroaa>2.0.co;2
- Wang, E. Q., Meng, K., Xu, G., Li, T. M., Ren, J. W., Qiao, X., et al. (2018). Cenozoic two-stage obduction of the Indian subcontinent: On the interaction between the Indian Ocean, Tethyan and Eurasian plates. *Acta Pet. Sin.* 34 (7), 1867–1875. in Chinese.
- Wang, M., Shen, Z. K., Gan, W. J., Liao, H., Li, T. M., Ren, J. W., et al. (2008). GPS monitoring of temporal deformation of the Xianshuihe fault. *Sci. Chi. Ser. D-Earth Sci.* 51, 1259–1266. doi:10.1007/s11430-008-0095-3
- Wang, M., and Shen, Z. K. (2020). Present-day crustal deformation of continental China derived from GPS and its tectonic implications. *J. Geophys. Res. Solid Earth* 125 (2), 1–22. doi:10.1029/2019JB018774
- Wang, P., Song, X., Han, D., Zhang, Y., and Liu, X. (2010). A study of root water uptake of crops indicated by hydrogen and oxygen stable isotopes: A case in shanxi province, China. *Agric. Water Manag.* 97, 475–482. doi:10.1016/j.agwat.2009.11.008
- Xia, J. W., and Zhu, M. (2020). Study on tectonic characteristics and activity of middle section of Jinshajiang main fault zoon. *Yangtze River* 51 (5), 131–137. in Chinese.
- Xu, X. X., Ji, L. Y., Jiang, F. Y., and Zhang, W. T. (2020). Study on current activity features of Jinshajiang Fault Zone based on GPS and small earthquakes. *J. Geod. Geodyn.* 40 (10), 1062–1067. in Chinese. doi:10.14075/j.jgg.2020.10.013
- Yan, R., Woith, H., and Wang, R. (2014). Groundwater level changes induced by the 2011 Tohoku earthquake in China mainland. *Geophys. J. Int.* 199, 533–548. doi:10.1093/gji/ggu196
- Yan, Y. C., Liu, F. L., Guo, L. S., Zhou, X. C., Ouyang, S. P., Li, J. C., et al. (2021). Hydrogeochemical characteristics of the hot springs in the longmenshan fault zone. *J. Seismol. Res.* 44 (2), 96–110. in Chinese. doi:10.3969/j.issn.1000-0666.2021.02.005
- Yang, T. F., Wen, H. Y., Fu, C. C., Lee, H. F., Lan, T. F., Chen, A. T., et al. (2011). Soil radon flux and concentrations in hydrothermal area of the tatan volcano group, northern taiwan. *Geochem. J.* 45 (6), 483–490. doi:10.2343/geochemj.10144
- Yi, L., Qi, J. H., Li, X., Xu, M., Zhang, X., Zhang, Q., et al. (2021). Geochemical characteristics and Genesis of the high-temperature geothermal systems in the north section of the Sanjiang Orogenic belt in southeast Tibetan Plateau. *J. Volcanol. Geotherm. Res.* 414 (2021), 107244. doi:10.1016/j.jvolgeores.2021.107244
- Yin, A., and Harrison, T. M. (2003). Geologic evolution of the Himalayan-Tibetan orogen. *Annu. Rev. Earth Planet. Sci.* 28 (28), 211–280. doi:10.1146/annurev.earth.28.1.211
- Yuce, G., Italiano, F., and D'Alessandro, W. (2014). Origin and interactions of fluids circulating over the Amik Basin (Hatay-Turkey) and relationships with the hydrologic, geologic and tectonic settings. *Chem. Geol.* 388, 23–39. doi:10.1016/j.chemgeo.2014.09.006
- Zhang, C. S., Zhang, Y. C., and Wu, M. L. (2003). Study on relationship between earthquake and hydro-geochemistry of groundwater in southern part of North-South earthquake belt in China. *J. Geomechanics* 9 (1), 21–30. in Chinese.

Zhang, J., Li, W., Tang, X., Tian, J., Wang, Y., Guo, Q., et al. (2017). Geothermal data analysis at the high-temperature hydrothermal area in Western Sichuan. *Sci. China Earth Sci.* 08 (60), 1507–1521. doi:10.1007/s11430-016-9053-2

Zhang, M. L., Guo, Z., Xu, S., Barry, P. H., Sano, Y., Zhang, L., et al. (2021). Linking deeply-sourced volatile emissions to plateau growth dynamics in southeastern Tibetan Plateau. *Nat. Commun.* 12, 4157. doi:10.1038/s41467-021-24415-y

Zhang, W., Wang, G. L., Xing, L. X., and Zhao, J. (2019). Geochemical response of deep geothermal processes in the Litang region, Western Sichuan. *Energy Explor. Exploitation* 2 (37), 626–645. doi:10.1177/0144598718812550

Zhao, L. F., Xie, X. B., He, J. K., Tian, X., and Yao, Z. X. (2013). Crustal flow pattern beneath the Tibetan Plateau constrained by regional Lg-wave Q tomography. *Earth Planet. Sci. Lett.* 383, 113–122. doi:10.1016/j.epsl.2013.09.038

Zhou, X. C., Liu, L., Chen, Z., Cui, Y., and Du, J. (2017). Gas geochemistry of the hot spring in the Litang fault zone, Southeast Tibetan Plateau. *Appl. Geochem.* 79, 17–26. doi:10.1016/j.apgeochem.2017.01.022

Zhou, X. C., Wang, W. L., Li, L. W., JianMin, H., LanTian, X., ZhongPing, L., et al. (2020a). Geochemical features of hot spring gases in the Jinshajiang-Red River fault zone, Southeast Tibetan Plateau. *Acta Pet. Sin.* 36 (7), 2197–2214. (in Chinese). doi:10.18654/1000-0569/2020.07.18

Zhou, Z. H., Tian, L., Zhao, J., Wang, H., and Liu, J. (2020b). Stress-related pre-seismic water radon concentration variations in the Panjin observation well, China (1994–2020). *Front. Earth Sci. (Lausanne)*. 8. doi:10.3389/feart.2020.596283

Zhou, Z. H., Zhong, J., Zhao, J., Yan, R., Tian, L., and Fu, H. (2021). Two mechanisms of earthquake-induced hydrochemical variations in an observation well. *Water* 13 (17), 2385. doi:10.3390/w13172385

Zhu, J. S., Wang, X. B., Yang, Y. H., Fan, J., and Cheng, X. Q. (2017). The crustal flow beneath the eastern margin of the Tibetan Plateau and its process of dynamics. *Chin. J. Geophys.* 60 (6), 2038–2057. in Chinese. doi:10.6038/cjg20170602